(12)

DNA 4207T

ON THE EXCITATION OF AXIALLY SYMMETRIC MODES OF A CYLINDRICAL CAVITY FOR HIGH FLUENCE SGEMP SIMULATION

Mission Research Corporation
735 State Street
Santa Barbara, California 93101

OCTOBER 1977

Topical Report for Period October 1976—October 1977

CONTRACT No. DNA 001-77-C-0009

THIS WORK SPONSORED BY THE DEFENSE NUCLEAR AGENCY
UNDER RDT&E RMSS CODE B323077464 R99QAXEE50104 H2590D.

Prepared for
Director
DEFENSE NUCLEAR AGENCY
Washington, D. C. 20305

Destroy this report when it is no longer needed. Do not return to sender.

(18) DNA, SBIE (19) 4207T, AD-E300 088

UNCLASSIFIED

SECURITY CLASSIFICATION OF THIS PAGE (When Data Entered)

REPORT DOCUMENTATION PAGE

READ INSTRUCTIONS BEFORE COMPLETING FORM

1. REPORT NUMBER: DNA 4207T	2. GOVT ACCESSION NO.
3. RECIPIENT'S CATALOG NUMBER (9)	
4. TITLE (and Subtitle): (6) ON THE EXCITATION OF AXIALLY SYMMETRIC MODES OF A CYLINDRICAL CAVITY FOR HIGH FLUENCE SGEMP SIMULATION.	5. TYPE OF REPORT & PERIOD COVERED: Topical Report for Period Oct 76—Oct 77
	6. PERFORMING ORG. REPORT NUMBER: (14) MRC-R-302
7. AUTHOR(s): (10) Roger Stettner	8. CONTRACT OR GRANT NUMBER(s): (15) DNA 001-77-C-0209
9. PERFORMING ORGANIZATION NAME AND ADDRESS: Mission Research Corporation, 735 State Street, Santa Barbara, California 93101	10. PROGRAM ELEMENT, PROJECT, TASK AREA & WORK UNIT NUMBERS: (16) (12) Subtask R99QAXEE501-04
11. CONTROLLING OFFICE NAME AND ADDRESS: (11) Director, Defense Nuclear Agency, Washington, D.C. 20305	12. REPORT DATE: OCT 77; 13. NUMBER OF PAGES: 42
14. MONITORING AGENCY NAME & ADDRESS (if different from Controlling Office)	15. SECURITY CLASS (of this report): UNCLASSIFIED (12) 38p.
	15a. DECLASSIFICATION/DOWNGRADING SCHEDULE

16. DISTRIBUTION STATEMENT (of this Report)

Approved for public release; distribution unlimited.

17. DISTRIBUTION STATEMENT (of the abstract entered in Block 20, if different from Report)

18. SUPPLEMENTARY NOTES

This work sponsored by the Defense Nuclear Agency under RDT&E RMSS Code B323077464 R99QAXEE50104 H2590D.

19. KEY WORDS (Continue on reverse side if necessary and identify by block number)

SGEMP Simulation
Modal Excitation
Space-Charge-Limited SGEMP

20. ABSTRACT (Continue on reverse side if necessary and identify by block number)

This excitation of the axially symmetric modes of a cylindrical tank are considered for circumstances which approximate those of a highly space-charge-limited SGEMP situation. The amplitudes of excitation are discussed from both a general point of view and with specific reference to the Physics International tank used with the Owl II photon source.

DD FORM 1 JAN 73 1473 EDITION OF 1 NOV 65 IS OBSOLETE

UNCLASSIFIED

SECURITY CLASSIFICATION OF THIS PAGE (When Data Entered)

406 548

CONTENTS

		PAGE
ILLUSTRATIONS		2
SECTION		
1	INTRODUCTION	3
2	THEORY	5
	2.1 GENERAL RELATION	5
	2.2 BOUNDARY LAYER AND TRIANGULAR TIME HISTORY PARTICULARIZATION	7
3	RESULTS	11
	3.1 SOME GENERAL CONSIDERATIONS	11
	3.2 FIELD DISTRIBUTION AMONG MODES	15
	3.3 APPROXIMATE MODAL MAGNITUDES	30
4	SUMMARY AND CONCLUSIONS	31
REFERENCES		33
APPENDIX I		35

ILLUSTRATIONS

FIGURE		PAGE
1	$\frac{J_1(X_n Y)}{J_1^2(X_n)}$ vs. Y.	12
2	Modal time factor vs. T/τ_{np}.	13
3	Sum of modes vs. time, T = 1.0 NS, r = .35 m, z = 1.5 m.	19
4	Sum of modes vs. time, T = 2.5 NS, r = .35 m, z = 1.5 m.	20
5	Sum of modes vs. time, T = 5.0 NS, r = .35 m, z = 1.5 m.	21
6	Sum of modes vs. time, T = 7.5 NS, r = .35 m, z = 1.5 m.	22
7	Sum of modes vs. time, T = 9.0 NS, r = .35 m, z = 1.5 m.	23
8	Sum of modes vs. time, T = 1.0 NS, r = 2 m, z = 3.3 m.	24
9	Sum of modes vs. time, T = 2.5 NS, r = 2 m, z = 3.3 m.	25
10	Sum of modes vs. time, T = 5.0 NS, r = 2 m, z = 3.3 m.	26
11	Sum of modes vs. time, T = 7.5 NS, r = 2 m, z = 3.3 m.	27
12	Sum of modes vs. time, T = 9.0 NS, r = 2 m, z = 3.3 m.	28

SECTION 1

INTRODUCTION

When trying to simulate SGEMP in a vacuum tank, cavity resonances are almost always excited. Exciting these resonances may or maynot affect measurements made on objects within the tank. In this report we will be concerned with calculating the amplitudes of cylindrical cavity resonances under a special set of circumstances.

We shall consider circumstances which approximate severe space-charge limiting. The objective of these considerations will be to obtain an understanding of the excitation amplitudes, in general, as functions of the time and length parameters involved and also to provide some specific, relevant, theoretical computation for the experiments performed by Mission Research Corporation at Physics International.

In a simulation of SGEMP, in a tank, photons are allowed to impinge on an object within the tank. The photons cause photoelectrons to be ejected from the object and the tank walls. These photoelectrons form sources of electromagnetic fields; the tank walls and object are the boundaries for the electromagnetic fields. In reality the tank and the object are the system which has resonant modes.

In our calculations we take the point of view that the source currents are axially symmetric and that the presence of an object does not greatly effect the modes of the cavity.[3] We also assume that the sources can be separated into the product of a function depending only upon spatial variables and a function depending only upon time. In Section 2.1 we obtain

a general formula for the modal amplitude of the magnetic field under these assumptions.

Under conditions of severe space charge limiting the sources reduce to electric dipole moments in space. If the test object is a disk on which the dipole moment is uniform, the source of fields exists only at the edge of the disk where the dipole moment is discontinuous. In Section 2.2, using the formula developed in Section 2.1, we derive a formula for the modal amplitude, excited by one point of discontinuity, after the source currents have ceased. Modal excitation due to an arbitrarily shaped object could, however, be approximated as a sum of point discontinuities.

A discussion of the consequences stemming from the general form of the equations derived in Section 2.2, together with numerical evaluations is presented in Section 3. The tank dimensions used in these numerical evaluations are: tank radius equal to 2 meters and tank length equal to 6 meters. These dimensions are roughly equivalent to the Physics International simulation tank used with Owl II. Table 1 presents some of the periods for the modes of this tank. Graphs which should simplify modal excitation estimates, for an arbitrary tank, are also presented in Section 3.

The results and conclusions are summarized in Section 4.

SECTION 2

THEORY

2.1 GENERAL RELATION

In this section we derive the general relation which expresses the amplitude of a cylindrical cavity mode in terms of the position, magnitude and time history of the driving currents. We begin with Maxwell's equations for an axisymmetric situation. By a simple manipulation of these equations, the equations describing the fields, in cylindrical coordinates, become:

$$\frac{\partial}{\partial r}\left(\frac{1}{r}\frac{\partial}{\partial r}\,rB\right) + \frac{\partial^2 B}{\partial z^2} - \frac{1}{c^2}\frac{\partial^2 B}{\partial t^2} = g \ , \tag{2-1}$$

where

$$g = \frac{4\pi}{c}\left(\frac{\partial}{\partial r}J_z - \frac{\partial}{\partial z}J_r\right) \ , \tag{2-2}$$

and

$$\frac{1}{c}\frac{\partial E_r}{\partial t} = -\frac{4\pi}{c}J_r - \frac{\partial B}{\partial z} \ , \tag{2-3}$$

and also

$$\frac{1}{c}\frac{\partial E_z}{\partial t} = -\frac{4\pi}{c}J_z + \frac{1}{r}\frac{\partial}{\partial r}(rB) \ . \tag{2-4}$$

In the above equation a subscript z or r refers to the z or r cylindrical coordinates respectively; E and B refer to the electric and magnetic fields respectively; and J refers to the spatial current density. If Equations 2-1 through 2-4 are to be satisfied in a conducting cavity (E fields parallel to the conducting surfaces are zero), $0 \le r \le R$, $0 \le z \le L$ then

$$B(r,z,t) = \sum_{n=1}^{\infty} \sum_{p=1}^{\infty} B_{np}(t) J_1\left(\frac{X_n}{R} r\right) \cos\left(\frac{p\pi z}{L}\right), \qquad (2\text{-}5)$$

and

$$g(r,z,t) = \sum_{n=1}^{\infty} \sum_{p=1}^{\infty} g_{np}(t) J_1\left(\frac{X_n}{R} r\right) \cos\left(\frac{p\pi z}{L}\right), \qquad (2\text{-}6)$$

where J_1 are Bessel functions of order one and

$$B_{np}(t) = 4(R^2 L J_1^2(X_n))^{-1} \int_0^R r\,dr \int_0^L dz B J_1\left(\frac{X_n}{R} r\right) \cos\left(\frac{p\pi z}{L}\right), \qquad (2\text{-}7)$$

$$g_{np}(t) = 4(R^2 L J_1^2(X_n))^{-1} \int_0^R r\,dr \int_0^L dz g J_1\left(\frac{X_n}{R} r\right) \cos\left(\frac{p\pi z}{L}\right), \qquad (2\text{-}8)$$

$$\frac{\partial}{\partial r}\left(r J_1\left(\frac{X_n}{R} r\right)\right)\Big|_{r=R} = 0 . \qquad (2\text{-}9)$$

In Equations 2-7 and 2-8 we have used the normalization relationship for the Bessel functions I-10, where KR in relation I-10 is replaced by the root X_n. The roots, X_n, are found from the boundary condition Equation 2-9.

We now need to find $B_{np}(t)$ in terms of $g_{np}(t)$ to solve the problem. Substituting Equations 2-5 and 2-6 into Equation 2-1 we have

$$\frac{\partial^2 B_{np}}{\partial t^2} + \omega_{np}^2 B_{np} = - c^2 g_{np} , \qquad (2\text{-}10)$$

where

$$\omega_{np}^2 = c^2 \left[\left(\frac{X_n}{R}\right)^2 + \left(\frac{p\pi}{L}\right)^2\right] . \qquad (2\text{-}11)$$

Equation 2-10 can be solved to yield

$$B_{np}(t) = \frac{c^2}{\omega_{np}} \int_0^t g_{np}(t') \sin \omega_{np}(t'-t)dt' , \qquad (2\text{-}12)$$

where we assume that $g(t) = 0$ for $t \leq 0$. Combining Equations 2-2, 2-8 and 2-12 we obtain the equation we are seeking:

$$B_{np}(t) = \frac{16\pi c}{R^2 L J_1^2(X_n)\omega_{np}} \int_0^t dt' \int_0^R r dr \int_0^L dz \Big[$$

$$\sin(\omega_{np}(t'-t) J_1(X_n r/R) \cos(p\pi z/L) \left(\frac{\partial}{\partial r} J_z - \frac{\partial}{\partial z} J_r\right)\Big] . \qquad (2\text{-}13)$$

2.2 BOUNDARY LAYER AND TRIANGULAR TIME HISTORY PARTICULARIZATION

Having obtained the general relation describing the amplitude of a cylindrical cavity mode as a function of time, for a general driving current, we calculate the amplitude for a circumstance which represents the setting up of a boundary layer on a disk. The disk has a radius r_0 and is located at the position z_0. The axis of the disk corresponds to the axis of the cavity. The spatial currents are idealized as

$$J_r = 0 , \qquad (2\text{-}14)$$

$$J_z = \sigma_0 \lambda \, \delta(z-z_0) H(r_0-r) \delta(t) , \qquad (2\text{-}15)$$

where we first use a very simple time history,

$$S(t) \equiv \frac{2}{T^2} t \quad 0 < t < T ,$$

$$S(t) = 0 \quad 0 > t > T , \qquad (2\text{-}16)$$

In Equation 2-15 λ represents a length characteristic of the boundary layer thickness; σ_0 represents a characteristic surface charge density for the boundary layer and T represents the time it takes to set up the boundary layer; δ and H are a delta function and a step function respectively. We next substitute Equations 2-14 through 2-16 into Equation 2-13 and perform the specified integrations.

The r and z integrations are as follows:

$$\int_0^L dz \int_0^R dr\ r\left(\frac{\partial}{\partial r} J_z - \frac{\partial}{\partial z} J_r\right)\cos(p\pi z/L)J_1 = -\sigma_0\lambda r_0 S(t)J_1\left(\frac{X_n}{R} r_0\right)\cos(p\pi z_0/L). \quad (2\text{-}17)$$

The integration over time is, for $t > T$

$$\int_0^T S(t')\sin(\omega_{np}(t'-t))dt' = -\frac{1}{\omega_{np}}\int_0^T S(t')\ \frac{\partial}{\partial t'}\cos(\omega_{np}(t'-t)dt'$$

$$= \frac{1}{\omega_{np}}\int_0^T \frac{\partial}{\partial t'} S(t)\cos(\omega_{np}(t'-t)dt' ,$$

$$= -\frac{1}{\omega_{np}^2}\int_0^T \frac{\partial^2}{\partial t'^2} S(t')\sin(\omega_{np}(t'-t))dt' ,$$

$$= \frac{2}{(T\omega_{np})^2}\left(\sin(\omega_{np}t)-\sin(\omega_{np}(t-T)\right) , \quad (2\text{-}18)$$

since

$$\frac{\partial^2}{\partial t^2} S(t) = \frac{2}{T^2}\left(\delta(0) - \delta(t-T)\right) . \quad (2\text{-}19)$$

We further reduce Equation 2-18 by using the formula for the addition of sine functions

$$\sin(\omega_{np}t)-\sin(\omega_{np}(t-T)) = 2\cos(\omega_{np}(t-T/2))\sin(\omega_{np}T/2) . \quad (2\text{-}20)$$

Substituting Equation 2-20 into 2-18 we have

$$\int_0^T S(t')\sin(\omega_{np}(t'-t))dt' = \left(\frac{2}{T\omega_{np}}\right)^2 \cos\omega_{np}(t-T/2)(\sin(\omega_{np}T/2)) . \quad (2\text{-}21)$$

Using Equations 2-17 and 2-21 in 2-13 we have

$$B_{np}(t) = \frac{64\pi c\rho_0 \lambda r_0}{R^2 L J_1^2(X_n) T^2 \omega_{np}^3} (\sin\omega_{np} T/2)$$

$$(J_1(X_n r_0/R)\cos(p\pi z_0/L)\cos(\omega_{np}(t-T/2)) \quad . \qquad (2\text{-}22)$$

Using

$$\omega_{np} = 2\pi/\tau_{np} \quad , \qquad (2\text{-}23)$$

where τ_{np} is the period of the mode described by the subscripts np, we can express Equation 2-22 as

$$B_{np}(t) = \sigma_0\left(\frac{8}{\pi^2}\right)\left(\frac{\lambda}{L}\right)\left(\frac{r_0}{R}\right)\left(\frac{cT}{R}\right)\left(\frac{\tau_{np}}{T}\right)^3 \left(\sin\left(\pi \frac{T}{\tau_{np}}\right)\right)$$

$$\left(\frac{J_1(X_n r_0/R)}{J_1^2(X_n)}\right)(\cos(p\ z_0/L))\cos(\omega_{np}(t-T/2)) \qquad (2\text{-}24)$$

If we had defined S(t) by a pulse which rises in T and decays to zero in 2T,

$$S(t) = \frac{1}{T^2} t \quad 0 < t < T \quad ,$$

$$S(t) = \frac{1}{T^2} (2T-t) \quad T < t < 2T \quad , \qquad (2\text{-}25)$$

$$S(t) = 0 \quad 2T < t \quad ,$$

we would have obtained Equation 2-24 with sin $(\pi T/\tau_{np})$ replaced by $\sin^2$ $(\pi T/\tau_{np})$ and $\cos(\omega_{np}(t-T/2))$ replaced by $-\sin(\omega_{np}(T-t))$. That is, with this new time history,

$$B_{np}(t) = \sigma_0\left(\frac{8}{\pi^2}\right)\left(\frac{\lambda}{L}\right)\left(\frac{r_0}{R}\right)\left(\frac{cT}{R}\right)\left(\frac{\tau_{np}}{T}\right)^3 \sin^2\left(\frac{\pi T}{\tau_{np}}\right)$$

$$\left(\frac{J_1(X_n r_0/R)}{J_1^2(X_n)}\right)(\cos(p\pi z_0/L))(\sin\omega_{np}(t-T)) \quad . \qquad (2\text{-}26)$$

The pulse defined by Equation 2-25 approximates the curve describing the time derivative of the dipole moment of a linear times exponential energy distribution with a linearly rising pulse.[2] [We will call the pulse described by Equations 2-16, pulse 1 and that described by Equation 2-25, pulse 2.] Since pulse 2 approximates a real physical situation, Equation 2-26 will be referred to more often than Equation 2-24. Pulse 1 is designed to indicate the effects of a very sharp, more pathological pulse. The actual pulse in Reference 2, page 29, Figure 23, does not really end as rapidly as the pulse described by Equations 2-25. Electrons escaping the boundary layer tend to lengthen the time over which the dipole moment changes. In our calculations we are not considering these electrons, since their effect may not be adequately treated by considering the boundary layer thickness to be small compared to the dimensions of the emitting object. In addition, real photon pulses may linearly rise for only a few boundary layer rise times; the photon pulse in Reference 2 rises continually.

The required Equation 2-24 expresses the amplitude of transverse magnetic modes described by the indices n and p in terms of the sources; $\sigma_0\lambda S(t)$ is the rate of change, with respect to time, of the dipole moment per unit area. Equations 2-18 and 2-19 show that the amplitude of the mode for these S(t), can be directly expressible in terms of the third derivative, with respect to time, of the dipole moment per unit area. In other words a contribution is made to the amplitude of a mode every time the slope of the S(t) curve changes. These changes can cancel each other. Such is the case when $T = \tau_{np}$ (see Equation 2-24 or 2-26).

SECTION 3

RESULTS

3.1 SOME GENERAL CONSIDERATIONS

Equation 2-24 and 2-26 describe the amplitude of the n,p mode after the driving current pulse is over. These expressions involve a factor which depends upon the roots X_n of the Bessel function J_0 and a factor which depends upon the ratio of the rise time to the period of the mode. These factors are plotted in Figures 1 and 2 respectively. Figures 1 and 2 can be used to estimate cavity modal responses. Figure 2 contains plots for the two S(t) discussed in Section 2. For small values of T/τ_{np} the curve describing pulse 1 goes as $\pi(\tau_{np}/T)^2$ and the curve describing pulse 2 goes as $\pi^2(\tau_{np}/T)$.

In Section 3.2 we will discuss the distribution of amplitudes of the n,p modes with respect to the amplitude of the lowest mode, n = 1, p = 0. We will now discuss how the amplitude of the modes depend upon the various parameters in Equation 2-24 and 2-26. It is clear from both these equations that smaller values of T in general give rise to larger amplitudes, however in the limit that $\pi T << \tau_{np}$ the amplitude for the np mode with pulse 2 is independent of T. For the sharper pulse, pulse 1, the amplitude increases as T^{-1} for $T \to 0$. From Figure 2, for n = 1, the amplitude of the lowest mode is smallest for smaller values of r_0/R. In the limit that $X_n r_0/R \to 0$ the amplitude of np mode goes as $(r_0/R)^2$ (see Equation 2-24 and 2-26). Keeping the points of discontinuity close to the axis for a given tank will therefore reduce the amplitude of the lower n modes or alternatively

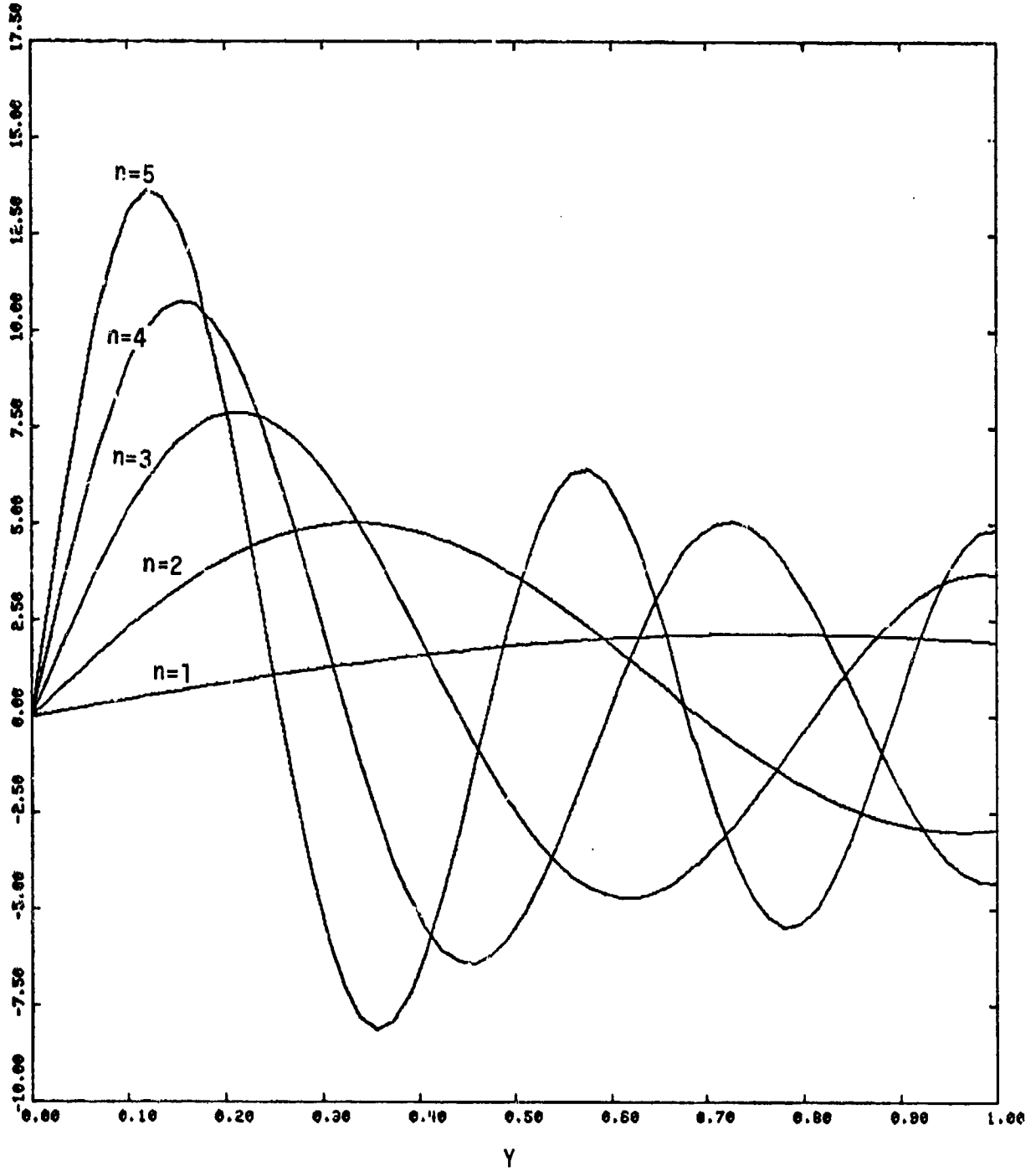

Figure 1. $\frac{J_1(X_n Y)}{J_1^2(X_n)}$ vs. Y.

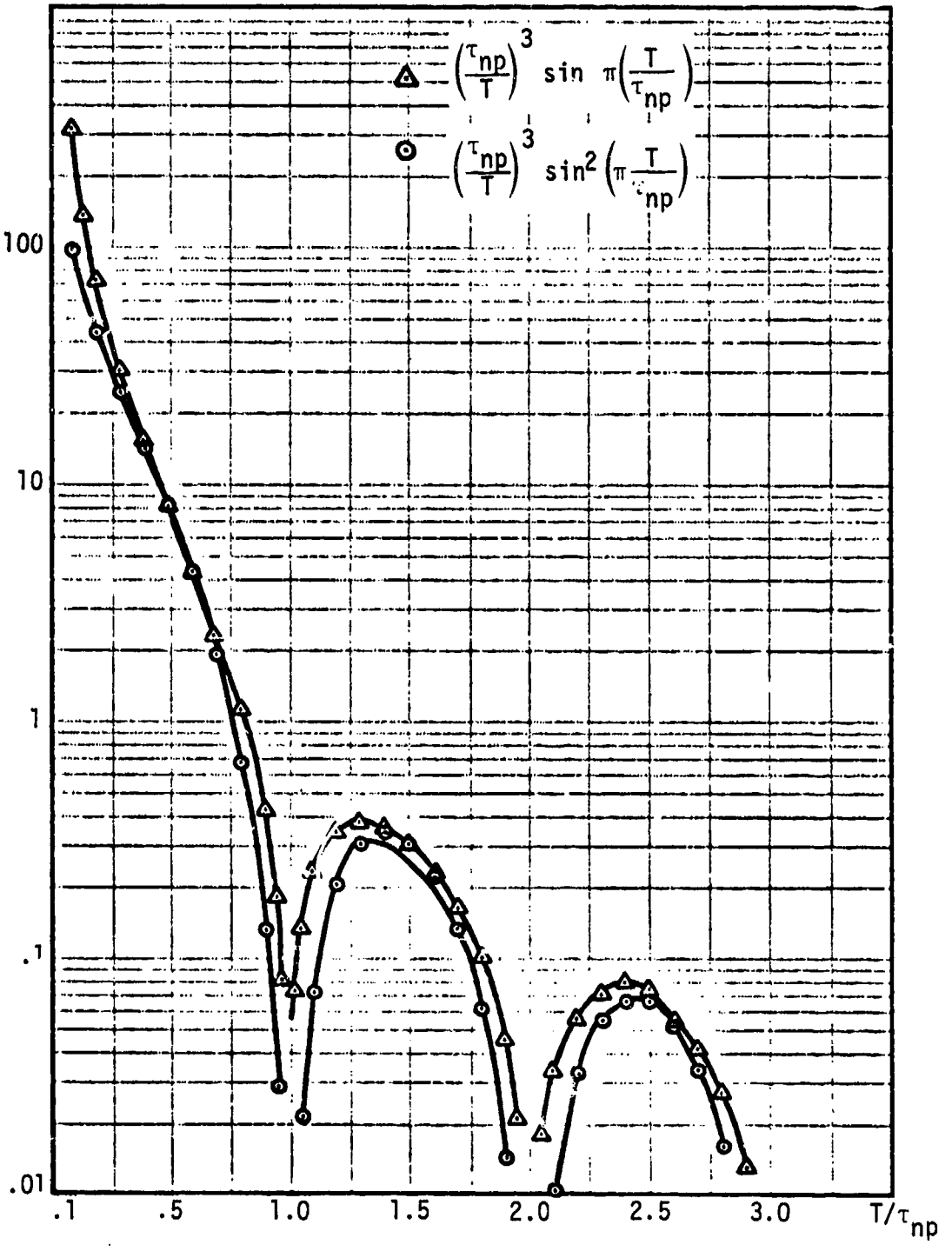

Figure 2. Modal time factor vs. T/τ_{np}.

increasing the radius of a tank, R, over the object size, r_0, will reduce the amplitudes of the modes like $(r_0/R)^2$.

We will now consider how the amplitudes depend upon the physics of the boundary layer. If we imagine that the modes are stimulated by a linearly rising photon pulse with a linear times exponential emission, electron energy distribution,then from Reference 2

$$\sigma_0\lambda = .417\ \bar{E}\ \frac{\text{statcoul}}{\text{cm}} \quad , \tag{3-1}$$

and

$$T = 1.28\ [\frac{\bar{E}^{1/2}}{Y\phi_0 f}]^{1/3}\ t_R^{2/3}\ \text{sec} \quad , \tag{3-2}$$

where $\bar{E}$ is the e-folding energy of the distribution (in keV), Y is the material yield (elect/cal), f is fraction of the energy in the rise of the photon pulse, t_R is the rise time of the photon pulse (in sec). The amplitude of the cavity modes depends upon the factor $\sigma_0\lambda/T^2$ (times a trigonometric function) which from Equations 3-1 and 3-2 is

$$\frac{\sigma_0\lambda}{T^2} \propto \left(\frac{\bar{E}Y\phi f}{t_R^2}\right)^{2/3} \quad . \tag{3-3}$$

The amplitude of the modal response is therefore more sensitive to the rise time of the photon pulse than it is to the other factors for $T \simeq T_{np}$. For $T_{np} >> T$ the amplitude of the modal response is proportional $\bar{E}$, with pulse 2; with pulse 1 the amplitude is proportional to $\bar{E}^{5/6}\ (Y\phi f/t_R^2)^{1/3}$. In other words for very short boundary layer rise times the average energy of the electrons is the more important quantity for stimulating the lower frequencies.

3.2 FIELD DISTRIBUTION AMONG MODES

It is important to understand what the relative amplitude of the modes are under various conditions, especially if one is interested in damping these modes. Tables 2 - 6 show the variation of modal distribution, normalized to the lowest mode, as T is varied from 1 NS to 9 NS, for pulse 2. Mode amplitudes are given for the modes $1 \leq n \leq 5$ and $0 \leq p \leq 9$. The tank parameters are: R = 2 m and L = 6 m. The position of the discontinuity is at r_0 = .5 m, z_0 = 1.5 m. These spatial parameters correspond to those of the "Disk" experiment performed by Mission Research Corporation (MRC) at Physics International in August of 1976. Table 1 gives the periods of the n,p modes for the given tank parameters.

It is worthwhile noting from Tables 2-6, that for a boundary layer rise time which is smaller than 2.5 NS some modes have amplitudes greater than the first mode. Combining the amplitudes of Tables 2-6 with the phase factors given in Equation 2-26 and inserting the result in Equation 2-5 we obtain Figures 3-7 and 8-12. Figures 3-7 are plots of the normalized magnetic field at r = .35 m, z = 1.5 m and Figures 8-12 are plots of the normalized B at r = 2 m and z = 3.3 m. These positions correspond, roughly, to two sensor positions in the MRC "Disk" experiment, one on the experimental object and the other on the tank wall. As the rise time of the boundary layer increases the lowest mode becomes more obvious as part of the "noise." The lowest mode appears to be more obvious at the tank wall position than at the position of the object.

We now examine the distribution of modes from a more general point of view. If $\overline{B}_{np}$ represents the amplitude of the np mode, then from Equation 2-26 for pulse 2, we have

Table 1. Modal periods.

τ_{np} in nanoseconds

	P = 0	1	2	3	4	5	6	7	8	9
N = 1	17.430	15.930	13.144	10.695	8.678	7.275	6.230	5.433	4.809	4.306
N = 2	7.593	7.460	7.100	6.599	6.046	5.509	5.012	4.568	4.178	3.838
N = 3	4.844	4.809	4.708	4.553	4.360	4.144	3.920	3.696	3.483	3.276
N = 4	3.555	3.541	3.500	3.435	3.350	3.249	3.137	3.019	2.898	2.777
N = 5	2.807	2.800	2.780	2.747	2.703	2.649	2.588	2.526	2.448	2.374

Tables 2 and 3. Ratio of modal amplitudes.

$\overline{B}_{np}/\overline{B}_{10}$

for τ = 1.00 NS z_0/L = 0.25 r_0/R = 0.25

P =	0	1	2	3	4	5	6	7	8	9
N = 1	1.000	0.547	0.000	-0.422	-0.482	-0.280	0.000	0.199	0.241	0.148
N = 2	1.814	1.258	0.000	-1.094	-1.393	-0.883	0.000	0.696	0.872	0.546
N = 3	1.741	1.210	0.000	-1.135	-1.514	-0.999	0.000	0.846	1.090	0.699
N = 4	0.982	0.690	0.000	-0.658	-0.893	-0.601	0.000	0.529	0.695	0.453
N = 5	0.093	0.066	0.000	-0.063	-0.087	-0.059	0.000	0.053	0.070	0.046

$\overline{B}_{np}/\overline{B}_{10}$

for τ = 2.50 NS z_0/L = 0.25 r_0/R = 0.25

P =	0	1	2	3	4	5	6	7	8	9
N = 1	1.000	0.640	0.000	-0.382	-0.482	-0.211	0.000	0.111	0.116	0.053
N = 2	1.435	0.963	0.000	-0.761	-0.892	-0.503	0.000	0.286	0.287	0.137
N = 3	0.836	0.557	0.000	-0.463	-0.559	-0.322	0.000	0.184	0.179	0.081
N = 4	0.179	0.124	0.000	-0.101	-0.119	-0.066	0.000	0.032	0.026	0.009
N = 5	0.002	0.001	0.000	-0.001	-0.001	0.000	0.000	0.000	0.000	0.000

Tables 4, 5 and 6. Ratio of modal amplitudes.

$\bar{B}_{np}/\bar{B}_{10}$ for τ = 5.00 NS z_0/L = 0.25 r_0/R = 0.25

P =	0	1	2	3	4	5	6	7	8	9
N = 1	1.000	0.614	0.000	-0.256	-0.189	-0.056	0.000	0.002	0.001	0.004
N = 2	0.453	0.291	0.000	-0.130	-0.088	-0.013	0.000	0.008	0.033	0.036
N = 3	0.003	0.003	0.000	-0.013	-0.036	-0.040	0.000	0.003	0.009	0.054
N = 4	0.079	0.056	0.000	-0.054	-0.072	-0.046	0.000	0.029	0.027	0.018
N = 5	0.002	0.002	0.000	-0.001	-0.001	0.000	0.000	0.000	0.000	0.000

$\bar{B}_{np}/\bar{B}_{10}$ for τ = 7.50 NS z_0/L = 0.25 r_0/R = 0.25

P =	0	1	2	3	4	5	6	7	8	9
N = 1	1.000	0.567	0.000	-0.105	-0.022	-0.001	0.000	0.019	0.021	0.006
N = 2	0.001	0.000	0.000	-0.036	-0.098	-0.004	0.000	0.047	0.023	0.001
N = 3	0.157	0.107	0.000	-0.076	-0.076	-0.023	0.000	0.000	0.013	0.022
N = 4	0.006	0.005	0.000	-0.010	-0.022	-0.020	0.000	0.024	0.028	0.012
N = 5	0.093	0.002	0.000	-0.001	-0.001	-0.001	0.000	0.000	0.000	0.000

$\bar{B}_{np}/\bar{B}_{10}$ for τ = 9.00 NS z_0/L = 0.25 r_0/R = 0.25

P =	0	1	2	3	4	5	6	7	8	9
N = 1	1.000	0.525	0.000	-0.033	-0.002	-0.024	0.000	0.017	0.003	0.001
N = 2	0.100	0.088	0.000	-0.139	-0.183	-0.001	0.000	0.000	0.013	0.026
N = 3	0.029	0.016	0.000	0.000	-0.005	-0.010	0.000	0.046	0.053	0.017
N = 4	0.052	0.030	0.000	-0.029	-0.051	-0.012	0.000	0.000	0.003	0.000
N = 5	0.001	0.001	0.000	-0.001	-0.002	-0.002	0.000	0.002	0.002	0.001

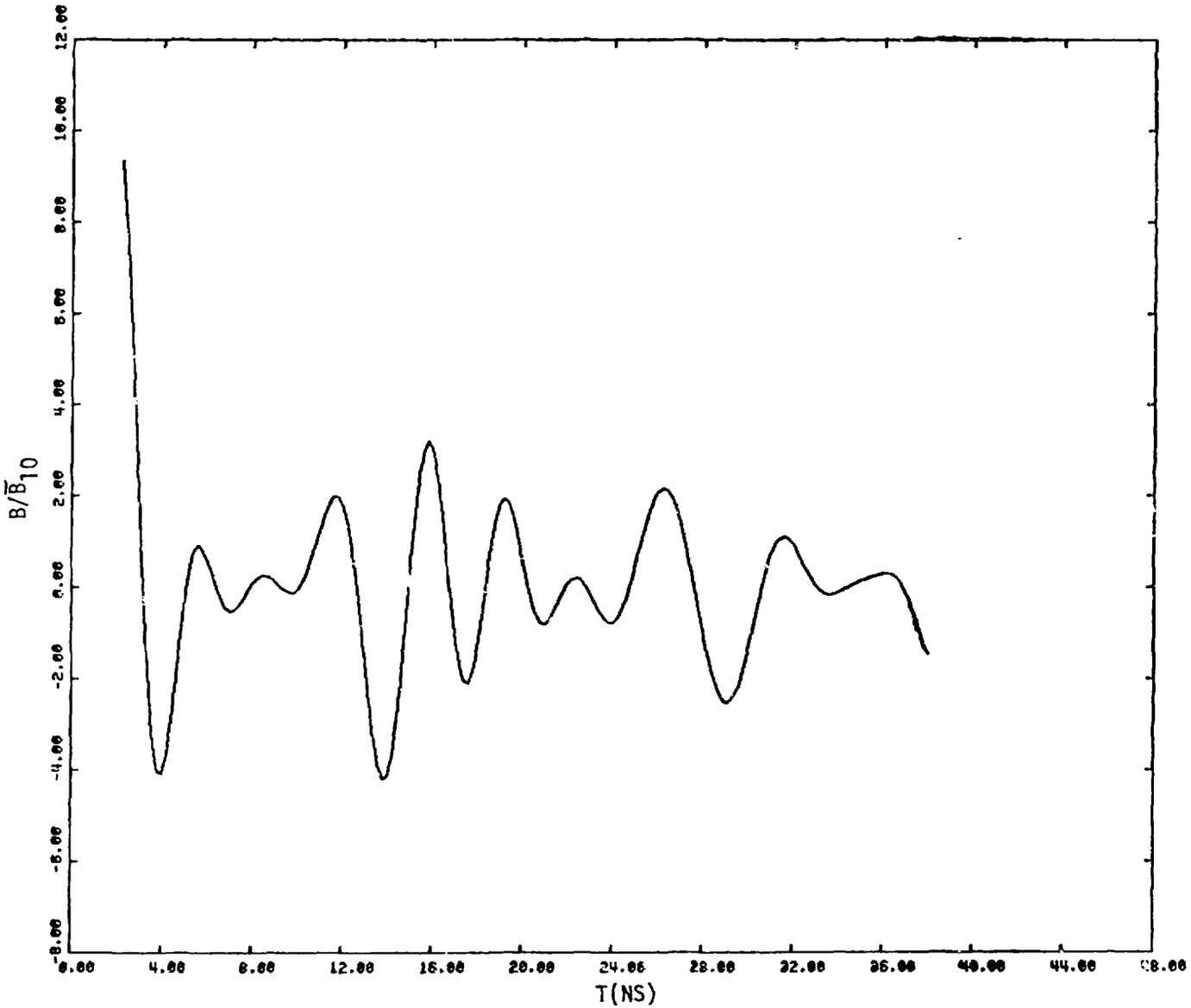

Figure 3. Sum of modes vs. time, T = 1.0 NS, r = .35 m, z = 1.5 m.

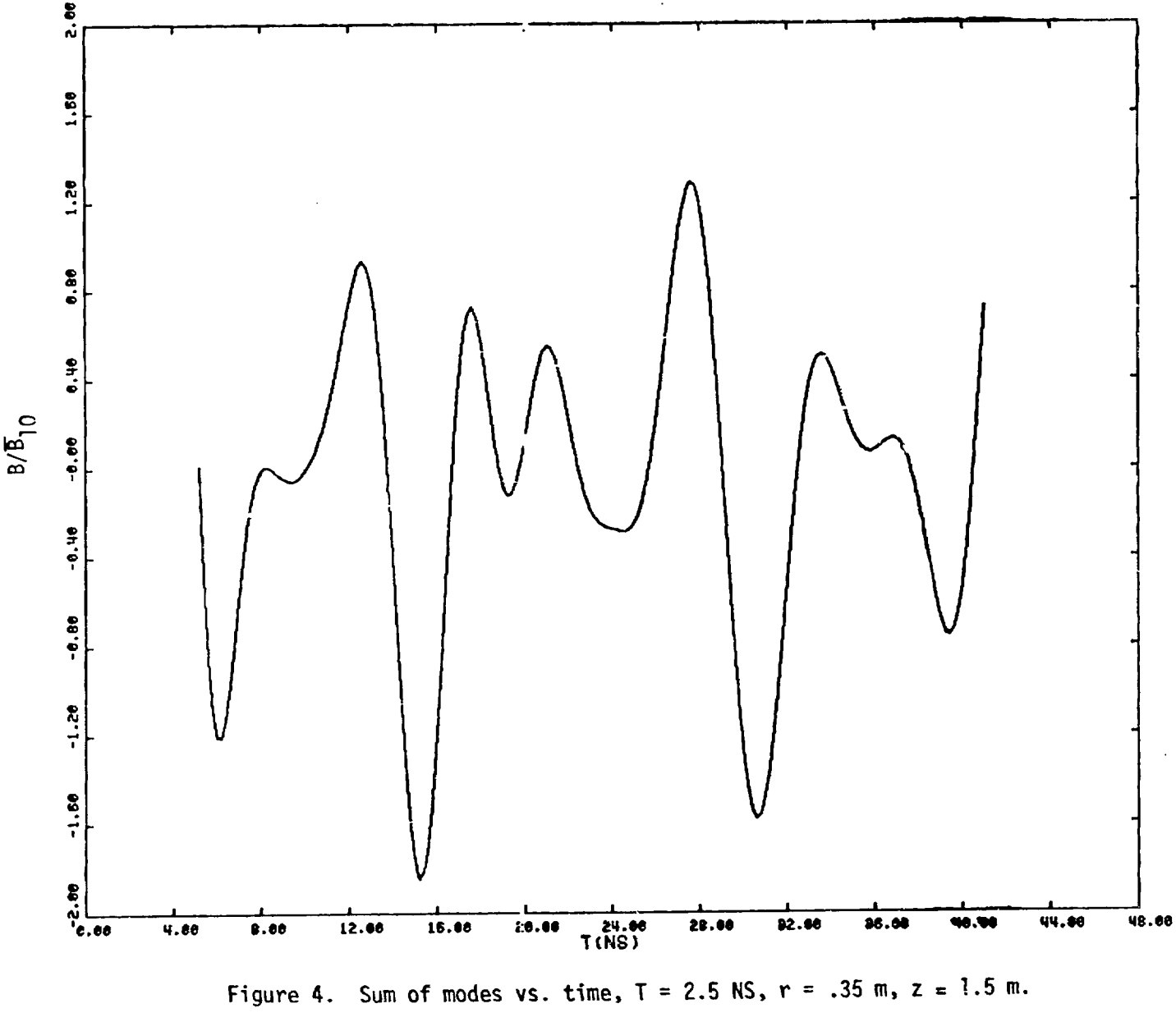

Figure 4. Sum of modes vs. time, T = 2.5 NS, r = .35 m, z = 1.5 m.

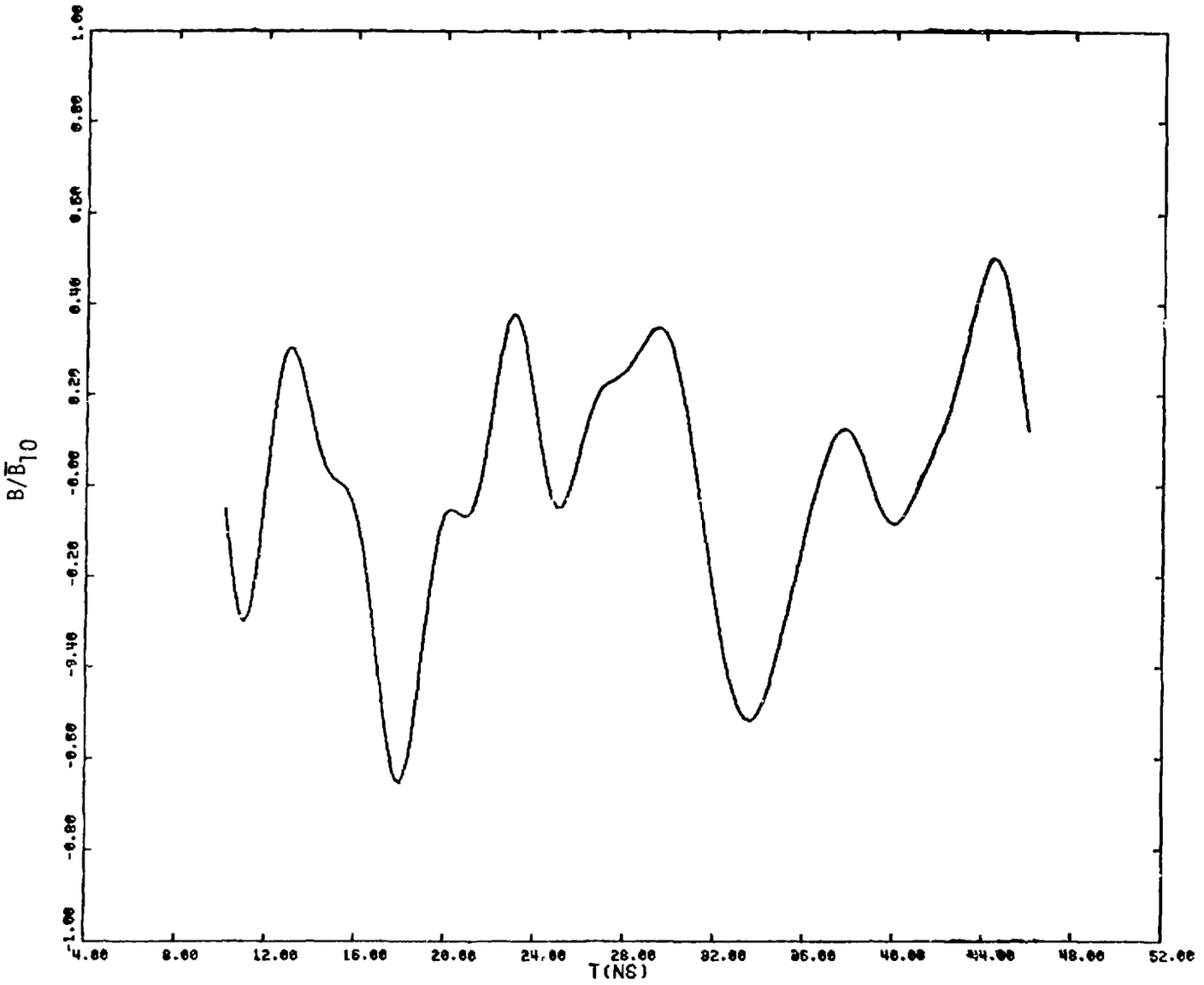

Figure 5. Sum of modes vs. time, $\bar{T}$ = 5.0 NS, r = .35 m, z = 1.5 m.

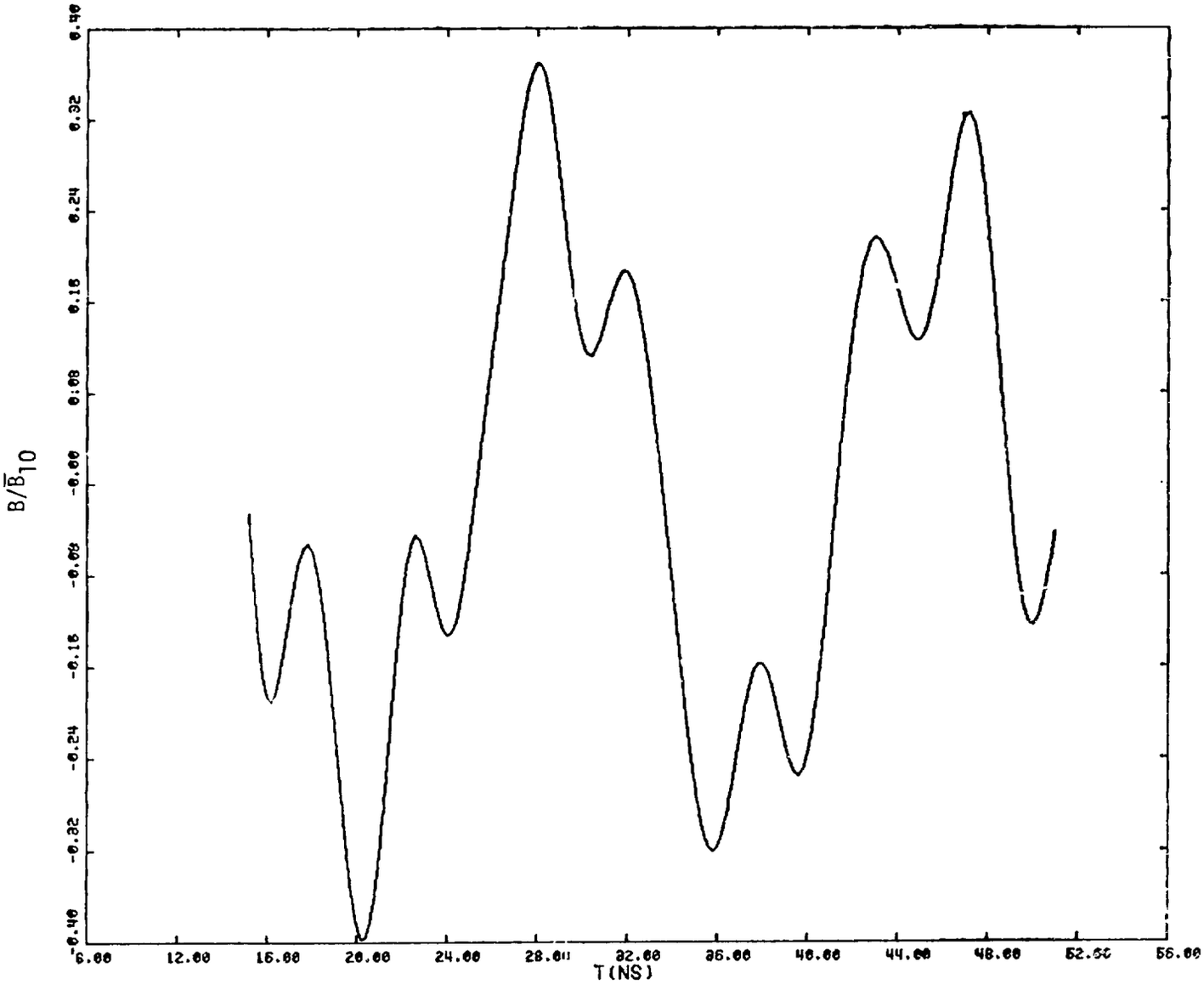

Figure 6. Sum of modes vs. time, T = 7.5 NS. r = .35 m, z = 1.5 m.

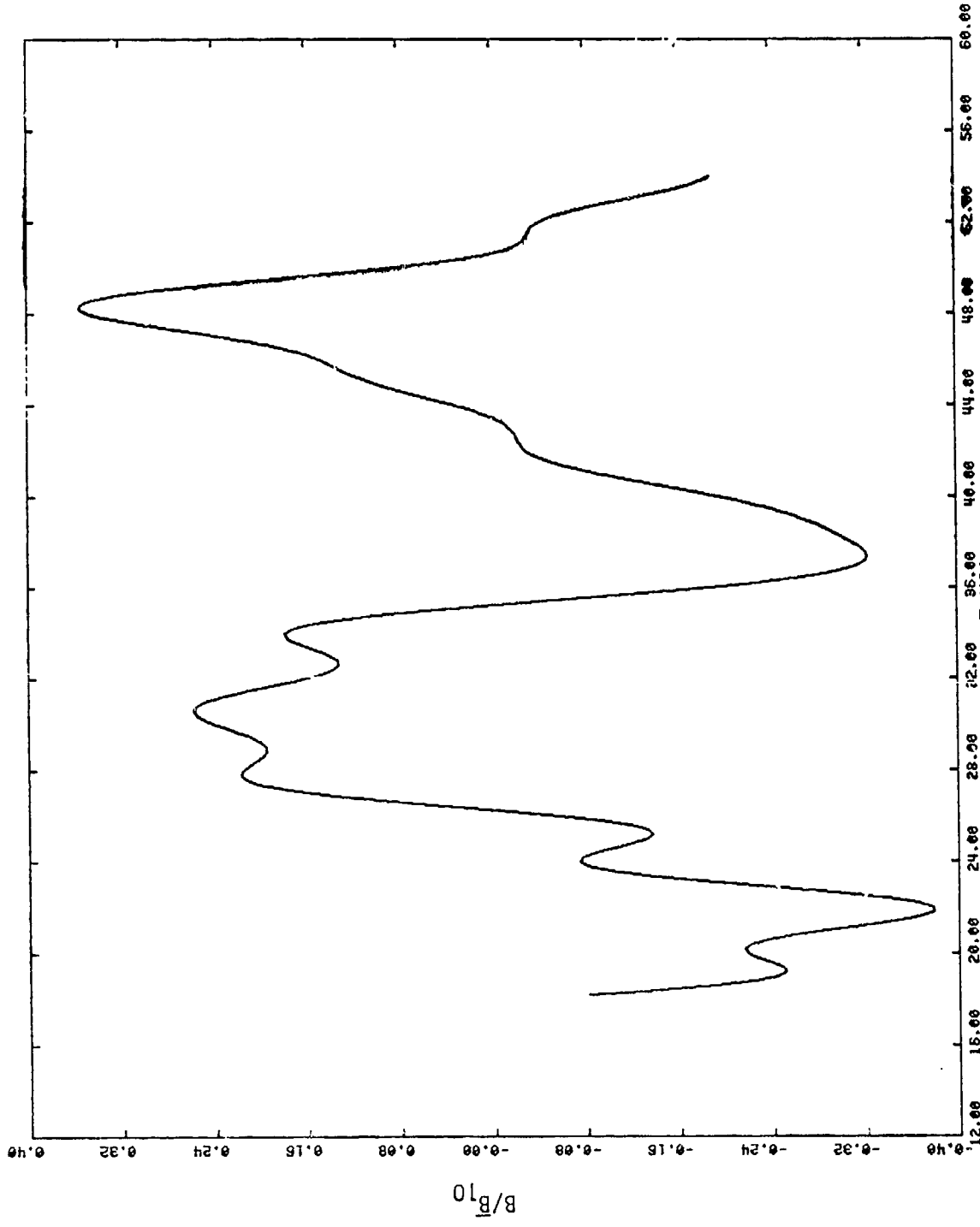

Figure 7. Sum of modes vs. time, T = 9.0 NS, r = .35 m, z = 1.5 m.

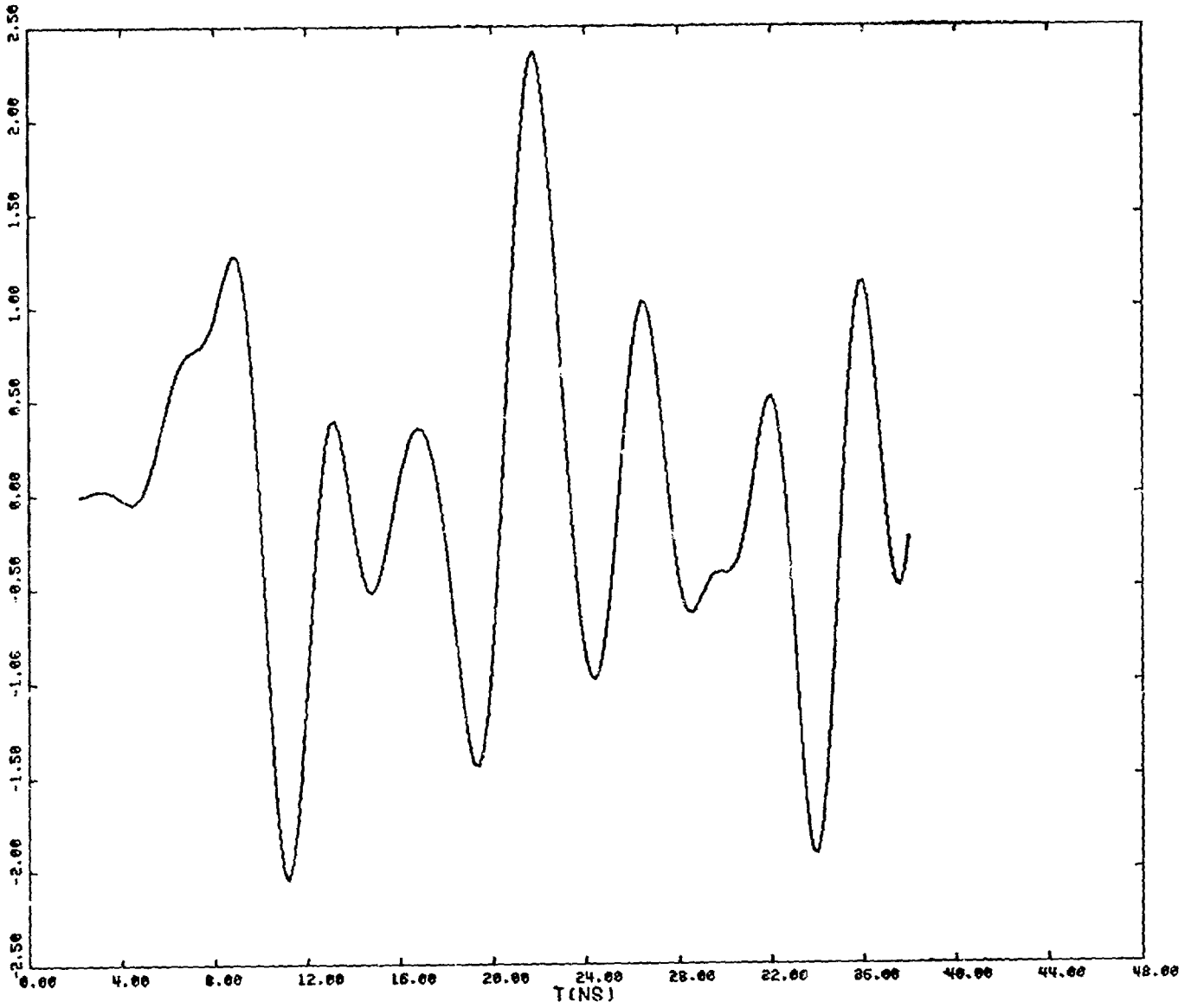

Figure 8. Sum of modes vs. time, T = 1.0 NS, r = 2 m, z = 3.3 m.

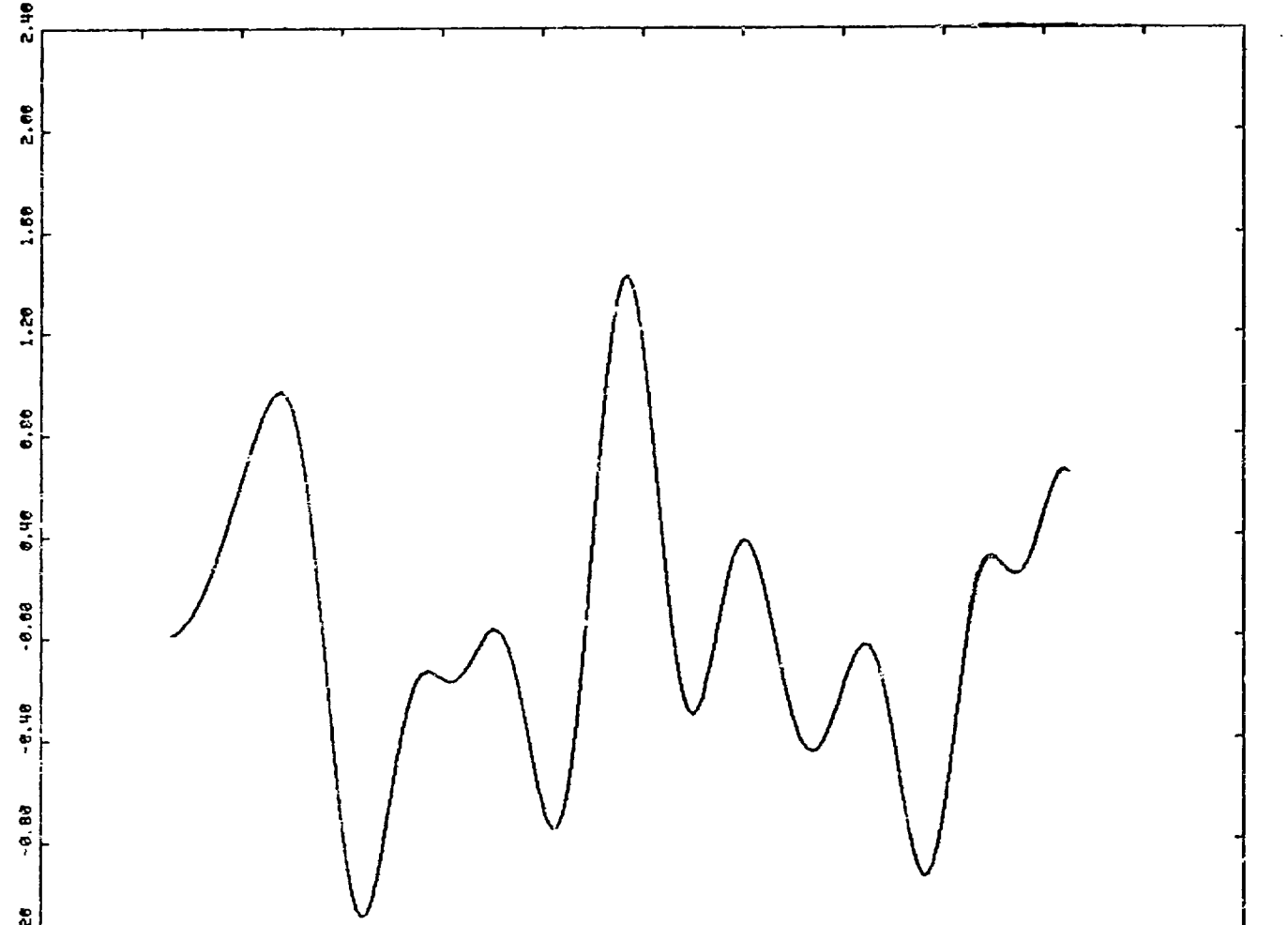

Figure 9. Sum of modes vs. time, T = 2.5 NS, r = 2 m, z = 3.3 m.

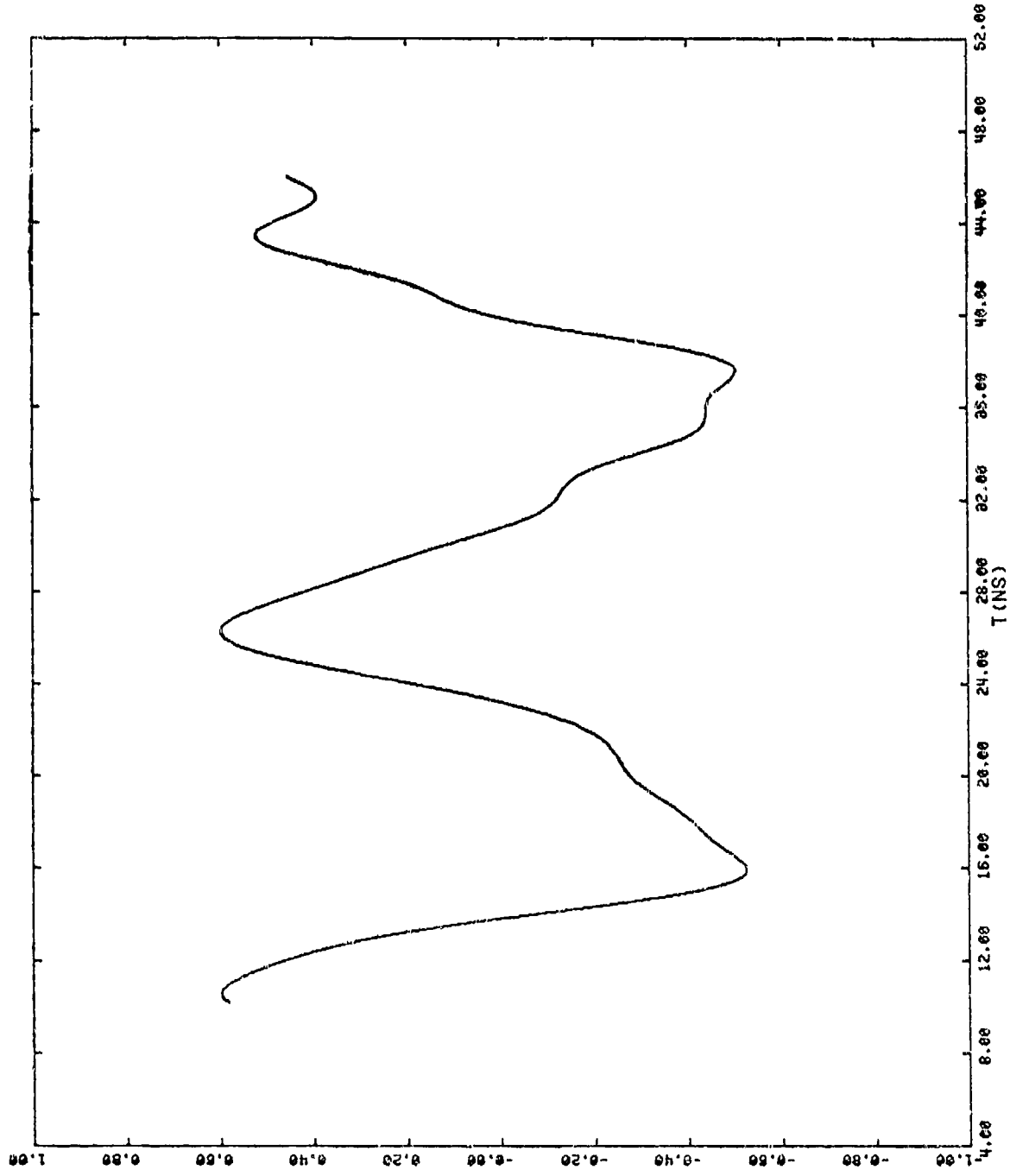

Figure 10. Sum of modes vs. time, T = 5.0 NS, r = 2 m, z = 3.3 m.

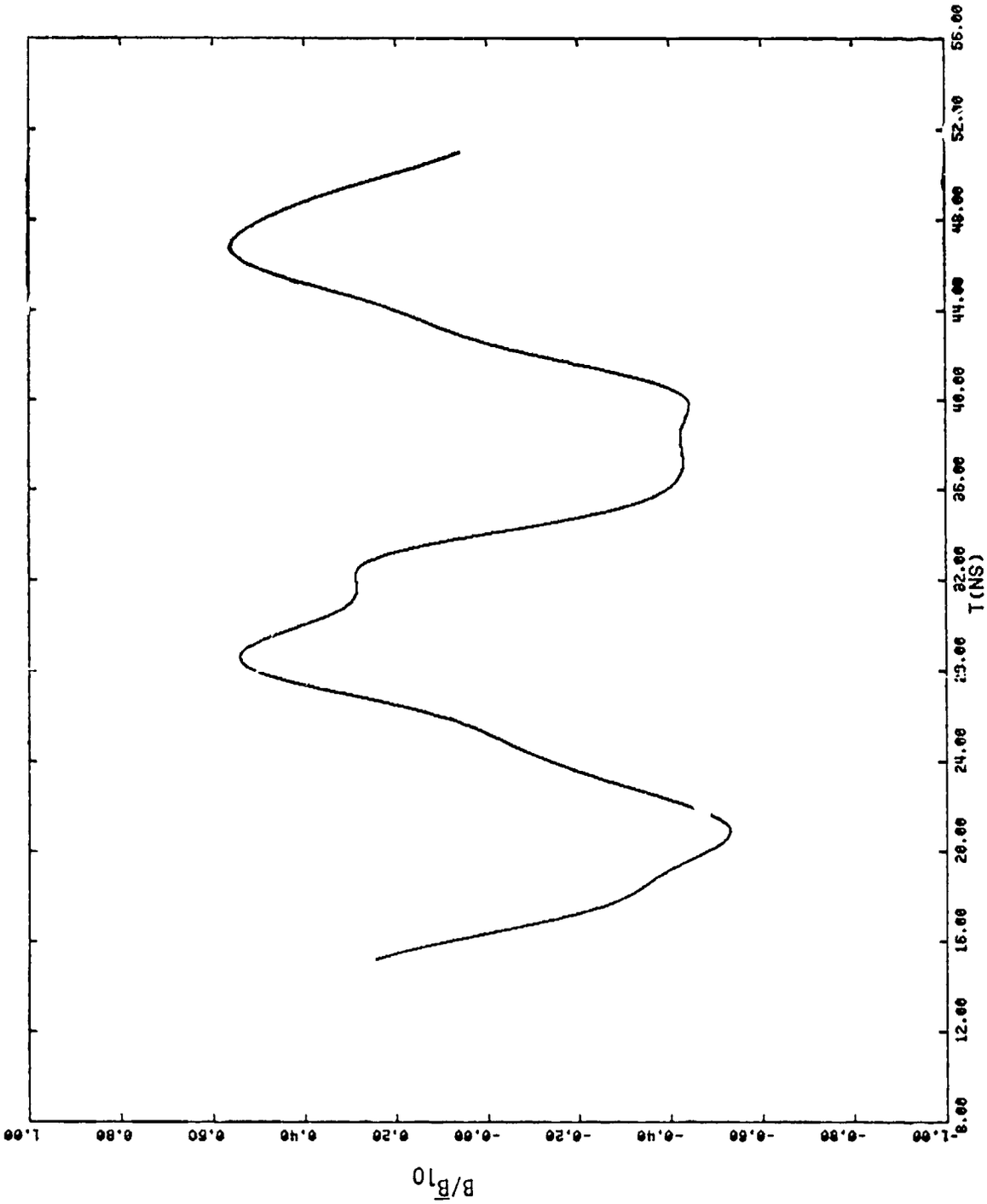

Figure 11. Sum of modes vs. time, T = 7.5 NS, r = 2 m, z = 3.3 m.

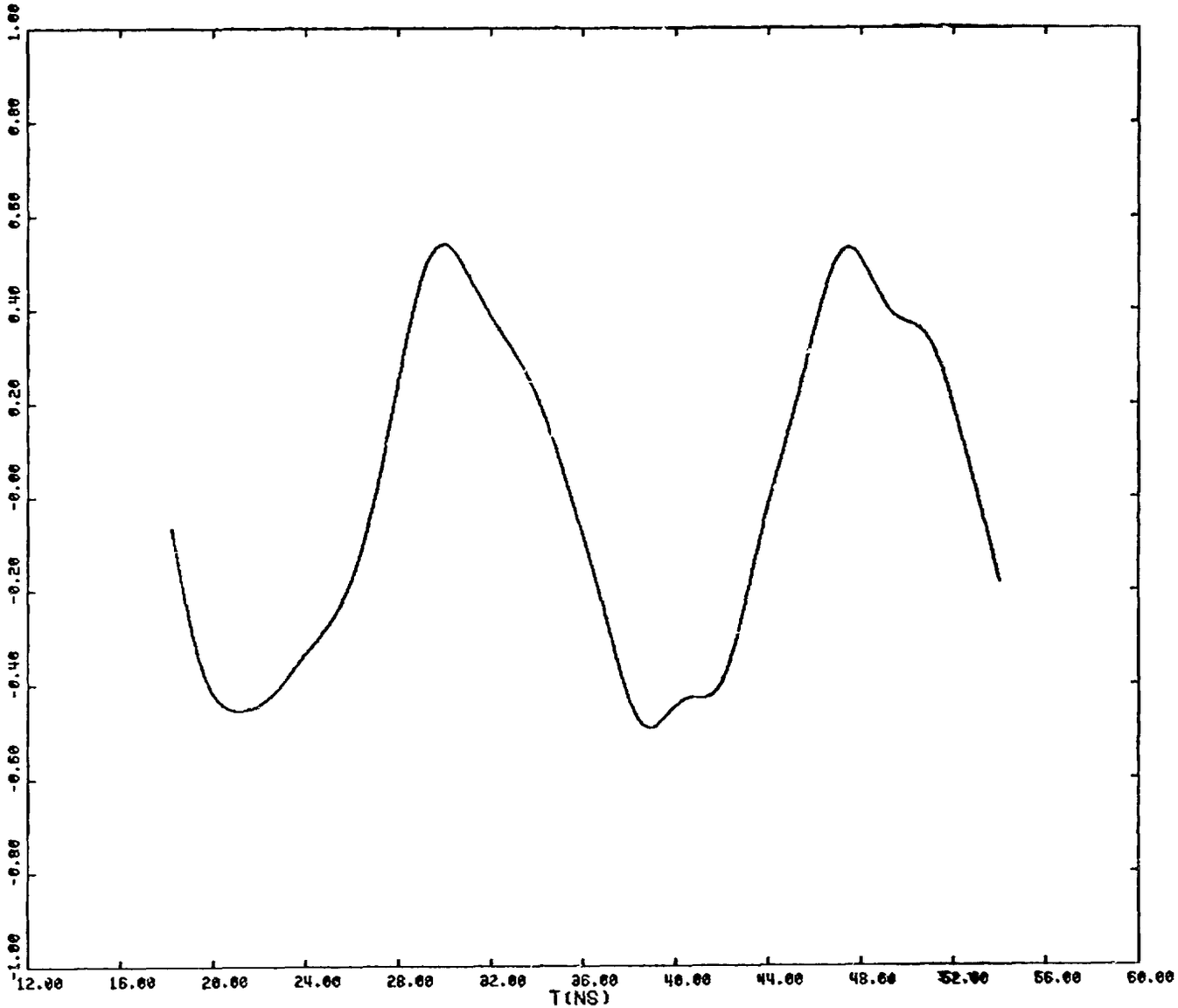

Figure 12. Sum of modes vs. time, T = 9.0 NS, r = 2 m, z = 3.3 m.

$$\frac{\bar{B}_{np}}{B_{10}} = \left(\frac{\tau_{np}}{\tau_{10}}\right)^3 \frac{\sin^2\left(\frac{\pi T}{\tau_{np}}\right)}{\sin^2\left(\frac{\pi T}{\tau_{10}}\right)} \frac{J_1(X_n \frac{r_0}{R})}{J_1(X_1 \frac{r_0}{R})} \frac{J_1^2(X_1)}{J_1^2(X_n)} \cdot$$

$$(\cos(p\pi \frac{z_0}{L})). \qquad (3\text{-}4)$$

Since $\tau_{10} > \tau_{np}$ it is clear from Equation 3-4 that smaller values of T favor larger relative amplitudes for the n,p modes. Smaller values of r_0/R, in general for a given n, also favor larger relative amplitudes for the n,p modes. For $r_0/R = 1$, the factor dependent upon r_0/R in Equation 3-4 is 1. For $r_0/R \to 0$, the factor dependent upon r_0/R in Equation 3-4 is equal to X_n/X_1, where $X_n > X_1$. (The factor dependent upon r_0/R goes through zero as r_0/R is varied between 1 and zero but the trend is for the extrema of the factor to increase as $r_0/R \to 0$. It should also be noted that $J_1^2(X_1)/J_1^2(X_n)$ is an increasing function of n so that for $T \ll \tau_{np}$ and $X_n\, r_0/R \ll 1$ Equation 3-4 becomes, with the help of Equation 2-11

$$\frac{\bar{B}_{np}}{B_{10}} \cong \frac{X_n}{\sqrt{X_n^2 + \left(\frac{R}{L}\pi p\right)^2}} \frac{J_1^2(X_1)}{J_1^2(X_n)} \cdot \qquad (3\text{-}5)$$

For $p = 0$ or $R/L \ll 1$ we have

$$\frac{\bar{B}_{np}}{\bar{B}_{10}} \cong \frac{J_1^2(X_1)}{J_1^2(X_n)} , \qquad (3\text{-}6)$$

that is under extreme conditions the higher n modes actually dominate, in a way specified by Equation 3-6, over the lowest mode, since $J_1(X_n) \leq J_1(X_1)$. The relative amplitude dependence on z position is given simply by the cosine function in Equation 3-4.

For a particular position within the tank the mode amplitudes continue to give rise to a total magnetic field through Equation 2-5. The extrema of $J_1(y)$ are a decreasing function of y so the general trend is for modes with larger n's to contribute less to the field as the tank wall is approached.

3.3 APPROXIMATE MODAL MAGNITUDES

We calculate the amplitude of the lowest mode (n = 1, p = 0) for T = 2.5 NS and T = 5 NS where $r_0/R = z_0/L = .25$. If $\bar{E} = .6$ keV then from Equation 3-1 $\sigma_0\lambda = .25$ statcoul/cm. For T = 2.5 NS, from Table 1 $T/\tau_{np} = .143$; for T = 5.0, from Table $T/\tau_{np} = .286$. Looking at Figure 2, for the pulse 2 curve, at these ratios we find that the time factor is about 60 and 25 respectively. We next look at Figure 1 for the Bessel function factor; it is about 1. Inserting the required number into Equation 2-24 we find that

$$\bar{B}_{10} \cong 2 \times 10^{-3} \text{ gauss} ,$$

for both values of T. Looking at Figures 3 and 4 we might expect the maximum B field of the noise to be about 4×10^{-3} to 1×10^{-3} gauss for T = 2.5 and T = 5.0 at the body sensor position. If the rise time of the boundary layer were only one nanosecond one might expect a peak noise magnetic field of about 10×10^{-3} gauss.

SECTION 4

SUMMARY AND CONCLUSIONS

In Section 2 an equation was derived which describes the modal excitation of a cylindrical cavity for a highly space-charge-limited situation; the space-charge dipole moment was uniform except at one point. A discussion of this equation was given in Section 3 together with some numerical evaluations. One of the time histories discussed in Section 3 approximated that of a detailed one-dimensional calculation. The one-dimensional calculation assumed a linear times exponential electron energy distribution and a linearly rising photon time history.

When the amplitude of the excited modes are expressed in terms of the boundary layer parameters it appears that, for boundary layer rise times which are larger than or roughly equal to a modal period, the rise time of the photon pulse is the most important parameter in exciting that mode. If the rise time of the boundary layer is much smaller than a modal period the average energy of the ejected electrons become the predominant factor in exciting that mode.

Qualitatively speaking, shorter boundary layer rise times favor larger amplitudes and increase the coupling to higher modes. As the rise time approaches zero, the distribution of amplitudes, relative to the lowest mode, approaches specified values independent of the rise time but dependent upon the position of the point of discontinuity of the dipole layer. These conclusions are what one generally expects but the equations in the text transform the general assertions into exact magnitudes.

As the rise time of the boundary layer decreases, the amplitudes of the modes become approximately independent of rise time for one case considered: that of a boundary layer whose electrons have a linear times exponential distribution. Again, qualitatively speaking, a point of dipole discontinuity close to the axis favors higher frequencies and smaller amplitudes. The amplitude of the lower modes, for a point of discontinuity close to the axis (or a small body in a large tank) goes roughly as the volume of the space-charge layer over the volume of the tank.

Determining the amplitude and distribution of modes is an important consideration in the simulation quality of any tank, especially if the modes must be damped. (Higher frequencies appear to be more easily damped than lower frequencies.) Numerical evaluation for spatial parameters relevant to the P.I. tank, and a range of boundary layer rise times indicate that the modal excitation is not always dominated by the lowest mode. A damper grid for this tank, to be used under severe space-charge limited circumstances, should be designed to be effective for a range of frequencies higher than the lowest mode.

In a simulation tank electrons emitted at the walls of the tank also contribute to modal stimulation. If these wall electrons are space charge limited then the equations in the text of this report can be used to estimate the amplitude of excitation of axisymmetric modes. The modal amplitude caused by a source discontinuity at the curved surface of the tank is less than for the optimum point of stimulation for that mode (the optimum point of discontinuity would occur at some radial point smaller than the radius of the tank); the distribution of modes for amplitudes stimulated at the curved surface of the tank tend to be towards the lower frequencies. The amplitude for a source continuity at the flat surfce of the tank is larger or equal to the amplitude stimulated by a discontinuity elsewhere in the axial direction.

REFERENCES

1. Jackson, J. D., Classical Electrodynamics, John Wiley and Sons, 1962.

2. Carron, N. J., Dynamical Solution of the SGEMP Boundary Layer for Linearly Rising and Constant X-ray Time Histories, Mission Research Corporation, MRC-R-300, December 1976.

3. Messier, M. A., The Effect of a Center Conductor on the Resonant Modes of a Spherical Cavity With a Perfectly Conducting Wall, Mission Research Corporation, Tank Physics Memo 5, September 1972.

OTHER RELEVANT WORK

Higgins, D. F., and C. L. Longmire, Cavity Mode Excitation, Mission Research Corporation, Tank Physics Memo 6, AFWL-TR-76-36, September 1972.

APPENDIX I

In this appendix we derive the normalization, for Bessel functions, used in the body of this report. Formulas for normalizing Bessel functions appear in the literature. However, these formulas are not always consistant from author to author. This short proof may satisfy the skeptic. The proof is designed to examine the boundary conditions which give rise to the normalization formula. We begin by obtaining a useful relation from Bessel's equation. Bessel's equation is

$$\frac{1}{r}\frac{d}{dr}\left(r\frac{d}{dr}J_n\right) + \left(K^2 - \frac{n^2}{r^2}\right)J_n = 0 \ . \qquad \text{(I-1)}$$

Multiplying Equation I-1 by $r^2 \frac{\partial}{\partial r} J_n$ and integrating, by parts, in the range $a \le r \le b$

$$\int_a^b dr r^2 J_n \frac{\partial}{\partial r} J_n = \frac{1}{2K^2}\left[\left(n^2 J_n^2 - r^2\left(\frac{\partial}{\partial r} J_n\right)^2\right)\right]_a^b \ , \qquad \text{(I-2)}$$

where we have used the fact that

$$\int_a^b dr J_n \frac{\partial J_n}{\partial r} = \frac{1}{2}\left[J_n^2\right]_a^b \ , \qquad \text{(I-3)}$$

and

$$\int_a^b dr\left(r\frac{\partial}{\partial r}J_n\right)\frac{\partial}{\partial r}\left(r\frac{\partial}{\partial r}J_n\right) = \frac{1}{2}\left[\left(r\frac{\partial}{\partial r}J_n\right)^2\right]_a^b \ . \qquad \text{(I-4)}$$

With Equation I-2 we are in a position to find the normalization constant. It is clear that

$$\frac{\partial}{\partial r}(rJ_n) = J_n + r\frac{\partial}{\partial r}J_n \quad . \tag{I-5}$$

Multiplying I-5 by rJ_n and integrating by parts over the range $a \leq r \leq b$ we find that

$$\int_a^b rJ_n^2 dr = \frac{1}{2}\left[r^2J_n^2 - \int_a^b drr^2J_n\frac{\partial}{\partial r}J_n\right] , \tag{I-6}$$

substituting Equation I-2 into I-6 we find that

$$rJ_n^2 dr = \frac{1}{2}\left[\left(r^2 - \left(\frac{n}{K}\right)^2\right)J_n^2 + \left(\frac{r}{K}\frac{\partial}{\partial r}J_n\right)^2\right]_a^b \quad . \tag{I-7}$$

For the normalization considered in this report:

$$\begin{aligned} a &= 0 \ , \\ b &= R \ , \\ n &= 1 \ ; \end{aligned} \tag{I-8}$$

and also for the boundary condition:

$$\frac{\partial}{\partial r}J_1\Big|_{r=R} = -\frac{J_1(KR)}{R} \quad , \tag{I-9}$$

we find upon substituting Equation I-8 and then I-9 into Equation I-7 that

$$\int_0^R rJ_1^2 dr = \frac{1}{2}\left(RJ_1(KR)\right)^2 \quad . \tag{I-10}$$

Equation I-10 is not the same as that found on page 73 of Reference 1, for example.

DISTRIBUTION LIST

DEPARTMENT OF DEFENSE

Director
Defense Advanced Rsch. Proj. Agency
ATTN: NMR

Director
Defense Communications Agency
ATTN: NMR

Defense Documentation Center
Cameron Station
12 cy ATTN: TC

Director
Defense Intelligence Agency
ATTN: DB-4C

Director
Defense Nuclear Agency
ATTN: TISI Archives
ATTN: DDST
2 cy ATTN: RAEV
3 cy ATTN: TITL Tech. Librar,

Commander, Field Command
Defense Nuclear Agency
ATTN: FCPR
ATTN: FCLMC

Director
Interservice Nuclear Weapons School
ATTN: Document Control

Director
Joint Strat. Tgt. Planning Staff, JCS
ATTN: JLTW-2

Chief
Livermore Division, Field Command, DNA
Lawrence Livermore Laboratory
ATTN: FCPRL

National Communications System
Office of the Manager
ATTN: NCS-TS

Director
National Security Agency
ATTN: R-425

OJCS/J-3
ATTN: J-3 RDTA Br. WWMCCS Plans Div.

OJCS/J-5
ATTN: J-5 Plans & Policy Nuc. Div.

Under Secretary of Def. for Rsch. & Engrg.
ATTN: S&SS (OS)

DEPARTMENT OF THE ARMY

Director
BMD Advanced Tech. Ctr.
Huntsville Office
ATTN: RDMH-O

DEPARTMENT OF THE ARMY (Continued)

Commander
BMD System Command
ATTN: BDMSC-TEN

Dep. Chief of Staff for Rsch. Dev. & Acq.
ATTN: DAMA-CSM-N

Commander
Harry Diamond Laboratories
ATTN: DRXDO-RCC, Raine Gilbert
ATTN: DRXDO-RCC, John A. Rosado
ATTN: DRXDO-TI, Tech. Lib.
ATTN: DRXDO-NP

Commander
Picatinny Arsenal
ATTN: SMUPA
ATTN: SARPA

Commander
Redstone Scientific Information Ctr.
U.S. Army Missile Command
ATTN: Chief, Documents

Chief
U.S. Army Communications Sys. Agency
ATTN: SCCM-AD-SV, Library

Commander
U.S. Army Electronics Command
ATTN: DRSEL

Commander
U.S. Army Foreign Science & Tech. Ctr.
ATTN: DRXST-ISI

DEPARTMENT OF THE NAVY

Chief of Naval Operations
ATTN: Code 604C3

Chief of Naval Research
ATTN: Henry Mullaney, Code 427

Director
Naval Research Laboratory
ATTN: Code 5410, John Davis
ATTN: Code 7701

Officer-In-Charge
Naval Surface Weapons Center
ATTN: Code WA501, Navy Nuc. Prgms. Off.

Director
Strategic Systems Project Office
ATTN: NSP

DEPARTMENT OF THE AIR FORCE

AF Geophysics Laboratory, AFSC
ATTN: Charles Pike

DEPARTMENT OF THE AIR FORCE (Continued)

AF Materials Laboratory, AFSC
ATTN: Library

AF Weapons Laboratory, AFSC
ATTN: SUL
2 cy ATTN: NTS
2 cy ATTN: JYC

Hq. USAF/RD
ATTN: RDQSM

Commander
Rome Air Development Center, AFSC
ATTN: Edward A. Burke

SAMSO/DY
ATTN: DYS

SAMSO/MN
ATTN: MNNH
ATTN: MNNG

SAMSO/SK
ATTN: SKF

SAMSO/XR
ATTN: XRS

Commander in Chief
Strategic Air Command
ATTN: XPFS
ATTN: NRI-STINFO Library

DEPARTMENT OF ENERGY

University of California
Lawrence Livermore Laboratory
ATTN: Tech. Info. Dept. L-3

Los Alamos Scientific Laboratory
ATTN: Doc. Con. for Reports Lib.

Sandia Laboratories
Livermore Laboratory
ATTN: Doc. Con. for Theodore A. Dellin

Sandia Laboratories
ATTN: Doc. Con. for 3141, Sandia Rpt. Coll.

OTHER GOVERNMENT AGENCY

NASA
Lewis Research Center
ATTN: Carolyn Purvis
ATTN: N. J. Stevens
ATTN: Library

DEPARTMENT OF DEFENSE CONTRACTORS

Aerospace Corporation
ATTN: Frank Hai
ATTN: Julian Reinheimer
ATTN: Library
ATTN: V. Josephson

Avco Research & Systems Group
ATTN: Research Lib., A830, Rm. 7201

DEPARTMENT OF DEFENSE CONTRACTORS (Continued)

The Boeing Company
ATTN: Preston Geren

University of California at San Diego
ATTN: Sherman de Forest

Computer Sciences Corporation
ATTN: Alvin T. Schiff

Dr. Eugene P. DePlomb
ATTN: Eugene P. DePlomb

Dikewood Industries, Inc.
ATTN: K. Lee
ATTN: Tech. Lib.

EG&G, Inc.
Albuquerque Division
ATTN: Tech. Lib.

Ford Aerospace & Communications Corp.
ATTN: Donald R. McMorrow, MS G30
ATTN: Library

General Electric Company
Space Division
Valley Forge Space Center
ATTN: Joseph C. Peden, VFSC, Rm. 4230M

General Electric Company
TEMPO-Center for Advanced Studies
ATTN: William McNamara
ATTN: DASIAC

Hughes Aircraft Company
ATTN: Tech. Lib.

Hughes Aircraft Company, El Segundo Site
ATTN: Edward C. Smith, MS A620
ATTN: William W. Scott, MS A1080

Institute for Defense Analyses
ATTN: IDA Librarian

IRT Corporation
ATTN: Dennis Swift
ATTN: Technical Library

Jaycor
ATTN: Library
ATTN: Eric P. Wenaas

Jaycor
ATTN: Robert Sullivan

Johns Hopkins University
Applied Physics Laboratory
ATTN: Peter E. Partridge

Kaman Sciences Corporation
ATTN: Library
ATTN: Jerry I. Lubell
ATTN: W. Foster Rich

Lockheed Missiles & Space Co., Inc.
ATTN: Dept. 85-85

DEPARTMENT OF DEFENSE CONTRACTORS (Continued)

McDonnell Douglas Corporation
ATTN: Stanley Schneider

Mission Research Corporation
ATTN: Roger Stettner
ATTN: Conrad L. Longmire
5 cy ATTN: Tech. Lib.

Mission Research Corporation-San Diego
ATTN: V. A. J. Van Lint
ATTN: Library

R&D Associates
ATTN: Leonard Schlessinger
ATTN: Technical Library

Rockwell International Corporation
ATTN: Technical Library

DEPARTMENT OF DEFENSE CONTRACTORS (Continued)

Science Applications, Inc.
ATTN: William L. Chadsey

Spire Corporation
ATTN: Roger G. Little

SRI International
ATTN: Library

Systems, Science and Software, Inc.
ATTN: Andrew R. Wilson
ATTN: Technical Library

TRW Defense & Space Sys. Group
ATTN: Tech. Info. Center/S-1930
2 cy ATTN: Robert M. Webb, R1-2410